



Dopant-Free Donor (D)- π -D- π -D Conjugated Hole-Transport Materials for Efficient and Stable Perovskite Solar Cells

Fei Zhang⁺,^[a, b, c] Xicheng Liu⁺,^[d] Chenyi Yi,^[b] Dongqin Bi,^[b] Jingshan Luo,^[b] Shirong Wang,^{*[a, c]} Xianggao Li,^{*[a, c]} Yin Xiao,^[a, c] Shaik Mohammed Zakeeruddin,^{*[b]} and Michael Grätzel^{*[b]}

Three novel hole-transporting materials (HTMs) using the 4-methoxytriphenylamine (MeOTPA) core were designed and synthesized. The energy levels of the HTMs were tuned to match the perovskite energy levels by introducing symmetrical electron-donating groups linked with olefinic bonds as the π bridge. The methylammonium lead triiodide (MAPbI₃) perovskite solar cells based on the new HTM Z34 (see main text for structure) exhibited a remarkable overall power conversion efficiency (PCE) of 16.1% without any dopants or additives, which is comparable to 16.7% obtained by a p-doped 2,2',7,7'-tetrakis-(*N,N*-di-4-methoxyphenylamino)-9,9'-spirobifluorene (spiro-OMeTAD)-based device fabricated under the same conditions. Importantly, the devices based on the three new HTMs show relatively improved stability compared to devices based on spiro-OMeTAD when aged under ambient air containing 30% relative humidity in the dark.

Increasing energy demands and concerns about global warming drive the exploration of clean, inexpensive, and renewable

energy sources. Recently, the photovoltaic community has witnessed a rapid emergence of a new class of solid-state heterojunction solar cells based on solution-processable organometal halide perovskite absorbers.^[1–3] The power conversion efficiency (PCE) of solid-state perovskite solar cells (PSCs) quickly increased to over 20%^[4–6] because of their unique characteristics, such as a broad spectral absorption range, large absorption coefficient, high charge carrier mobility, and long diffusion length.^[2]

In the configuration of a PSC, the hole transporting material (HTM) plays the key role of promoting hole migration, as well as preventing internal charge recombination.^[7] A great number of HTMs have been developed and applied in PSCs, including various newly designed, inorganic p-type semiconductors, conducting polymers, as well as small molecule hole conductors.^[8] 2,2',7,7'-Tetrakis(*N,N*-di-*p*-methoxyphenylamine)-9,9'-spirobifluorene (spiro-OMeTAD) that was well studied in solid state DSCs, continues to exhibit high performance in PSCs. Owing to its relatively low hole mobility and tedious synthesis strongly correlated to its production cost, numerous alternative HTMs have been explored with an aim to replace spiro-OMeTAD.^[9–20] Although inorganic HTMs (CuI and CuSCN) have drawn much attention because of their high hole mobility values and low production cost,^[21] polymeric HTMs, such as conjugated polytriarylamine (PTAA)^[22] and poly(3-hexylthiophene-2,5-diyl) (P3HT),^[23] have also shown competitive performances in PSCs, small molecular HTMs have advantages of their convenient purification, controllable molecular structures and relatively high efficiency.^[24] Regarding small molecule HTMs incorporated with dopants, the PCE of dopant-free HTM-based devices are consistently lying between 10 and 13%,^[25–36] but few are over 15%.^[37–40]

Herein, we report the synthesis and characterization of three novel dopant-free 4-methoxytriphenylamine (MeOTPA)-based HTMs as shown in Figure 1a, as well as their application in PSCs using methylammonium lead triiodide (CH₃NH₃PbI₃) perovskite. The energy levels of the HTMs can be tuned by substituting the MeOTPA core with different electron-donating groups through olefinic bonds. The device, fabricated with undoped Z34 as HTM, achieves a PCE of 16.1% under AM1.5G (100 mW cm⁻²) illumination. This result is comparable to that obtained using the well-known p-doped spiro-OMeTAD (16.7%). Moreover, the devices based on the three HTMs present improved stability compared with the device based on spiro-OMeTAD under ambient air with 30% relative humidity

[a] F. Zhang,⁺ Prof. S. Wang, Prof. X. Li, Dr. Y. Xiao
School of Chemical Engineering and Technology
Tianjin University
300072 Tianjin (China)
E-mail: wangshirong@tju.edu.cn
lixianggao@tju.edu.cn

[b] F. Zhang,⁺ Dr. C. Yi, Dr. D. Bi, Dr. J. Luo, Dr. S. M. Zakeeruddin,
Prof. M. Grätzel
Laboratory of Photonics and Interfaces,
Institute of Chemical Sciences and Engineering
École Polytechnique Fédérale de Lausanne (EPFL)
Station 6 CH-1015, Lausanne (Switzerland)
E-mail: shaik.zakeer@epfl.ch
michael.gratzel@epfl.ch

[c] F. Zhang,⁺ Prof. S. Wang, Prof. X. Li, Dr. Y. Xiao
Collaborative Innovation Center of Chemical Science
and Engineering (Tianjin)
300072 Tianjin (China)

[d] X. Liu⁺
School of Chemistry and Chemical Engineering
Qufu Normal University
273165 Qufu (China)

[⁺] These authors contributed equally to this work.

Supporting Information for this article can be found under:
<http://dx.doi.org/10.1002/cssc.201600905>.

This publication is part of a Special Issue focusing on the "Stability of Perovskite Solar Cells & Devices". To view the Complete issue, visit:
<http://onlinelibrary.wiley.com/doi/10.1002/cssc.v9.18/issuetoc>.

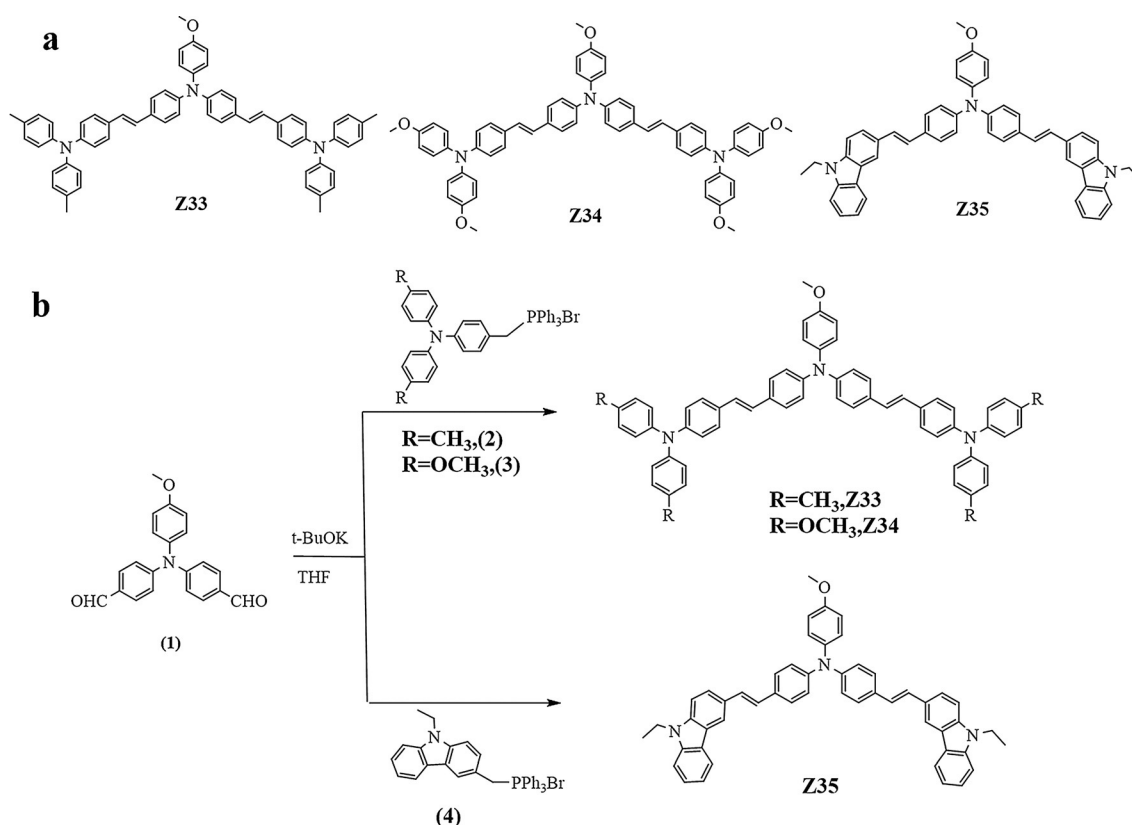


Figure 1. (a) Molecular structures of three HTMs; (b) synthetic route for three HTMs.

without encapsulation after storing the device for 1000 h in the dark. The synthetic cost of the new HTMs is around 1/10 of that required for spiro-OMeTAD.

The MeOTPA-based HTMs were synthesized using a Wittig reaction with cheap starting materials. The synthetic route for the HTMs is depicted in Figure 1b and experimental details are given in the Experimental Section. The new MeOTPA derivatives (Z33, Z34, and Z35) were fully characterized by ^1H NMR spectroscopy, high resolution mass spectroscopy, and elemental analysis. All the analytical data are consistent with the proposed structures. All of the HTMs show good solubility in common organic solvents, such as dichloromethane, chloroform, tetrahydrofuran, and toluene. We also roughly estimated the synthetic cost of 1 g Z33, Z34, and Z35, and the details are shown in the Supporting Information. The estimated synthesis cost of Z33, Z34, and Z35 is $\$70\text{ g}^{-1}$, $\$66\text{ g}^{-1}$ and $\$54\text{ g}^{-1}$, respectively which is much cheaper than that of spiro-OMeTAD ($\$598\text{ g}^{-1}$).

The UV/Vis absorption spectra of Z33, Z34, and Z35 in tetrahydrofuran (THF) solution and as thin films are shown in Figure 2a, and the corresponding data are summarized in Table 1. As shown in Figure 2a, all of them show two absorption bands in the 300–320 nm and 400–450 nm regions. The absorption bands in the 300–320 nm region can be assigned to the $n\text{-}\pi^*$ transition of the TPA moieties. The absorption in the 400–450 nm range is attributed to the intramolecular charge transfer (ICT) $\pi\text{-}\pi^*$ transition.^[41] Owing to the smaller degree of

conjugation,^[42] the ICT peak ($\lambda_{\text{max}}^{\text{abs}}$) of Z35 shows a blue shift compared with Z33 and Z34.

Thermogravimetric analysis (TGA) and differential scanning calorimetry (DSC) measurements show that these three HTMs have high decomposition temperatures ($T_d=432.3$, 417.2, and 402.5°C for Z33, Z34, and Z35, respectively) and glass transition temperatures ($T_g=96.2$, 106.1, and 89.1°C for Z33, Z34, and Z35, respectively) (Figure S1a in the Supporting Information).

To understand the charge-carrier transport properties of these HTMs, their hole mobility values (μ_h) were determined from transit times (t_T , Figure S3) using the equation: $\mu = d^2/Vt_T$ ^[43] where d is the organic film thickness and V is the applied voltage. At room temperature, μ_h of Z33, Z34, and Z35 are 4.67×10^{-4} , 7.46×10^{-4} , and $2.76 \times 10^{-4}\text{ cm}^2\text{V}^{-1}\text{s}^{-1}$ under the electric field of $1.0 \times 10^5\text{ V cm}^{-1}$, respectively. All three new HTMs have higher μ_h than pristine spiro-OMeTAD ($1.76 \times 10^{-4}\text{ cm}^2\text{V}^{-1}\text{s}^{-1}$ at the electric field of $1.0 \times 10^5\text{ V cm}^{-1}$), which is consistent with previously reported data ($2 \times 10^{-4}\text{ cm}^2\text{V}^{-1}\text{s}^{-1}$ at the electric field of $2.6 \times 10^5\text{ V cm}^{-1}$).^[44]

Density functional theory (DFT) calculations were carried out to understand the electronic structure and energy levels of the HTMs. The optimized molecular geometries, the highest occupied molecular orbital (HOMO) levels, and the lowest unoccupied molecular orbital (LUMO) energy levels are shown in Figure S2. The LUMO is distributed mainly on the part of the peripheral units close to the triphenylamine core, whereas the

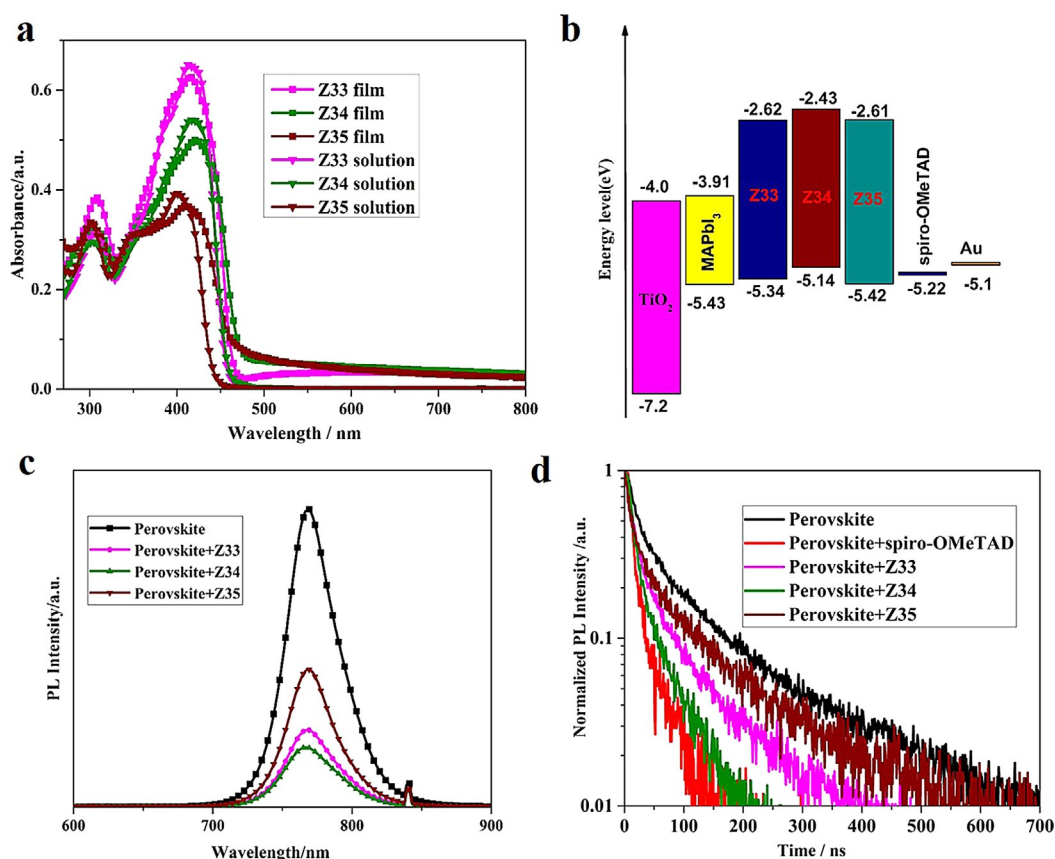


Figure 2. (a) UV/Vis absorption spectra of the HTMs in THF solution ($c = 1.0 \times 10^{-5} \text{ mol L}^{-1}$) and as films on glass; (b) energy level diagram of the corresponding materials used in PSCs; (c) photoluminescence (PL) spectra for different materials as films on glass; and (d) normalized time-resolved PL spectra of the corresponding samples.

HTM	$\lambda_{\text{max}}^{\text{abs}}$ [nm]		E_g [eV]	HOMO [eV]		LUMO [eV]		T_d [°C]	T_g [°C]	
	THF ^[a]	film ^[b]		exp. ^[c]	DFT ^[d]	exp. ^[e]	DFT ^[d]			exp. ^[f]
Z33	414	416	2.72	3.03	-5.34	-4.35	-2.62	-1.32	432.3	96.2
Z34	418	422	2.71	3.02	-5.14	-4.23	-2.43	-1.21	417.2	106.1
Z35	403	414	2.81	3.23	-5.42	-4.38	-2.61	-1.15	402.2	89.1

[a] UV/Vis absorption of THF solution ($c = 1.0 \times 10^{-5} \text{ mol L}^{-1}$). [b] UV/Vis absorption of the films. [c] Estimated from the onset of the long wavelength absorption in solution. [d] DFT theoretical calculation values. [e] Experimental HOMO values were measured by photoemission yield spectroscopy. [f] Experimental LUMO values were estimated using the following equation: $\text{LUMO} = \text{HOMO} + E_g$.

HOMO energy levels are distributed mainly on the central triphenylamine core and the extended vinyl π bridges. The calculated HOMO energy levels of the three HTMs are estimated to be -4.35, -4.23, and -4.38 eV for Z33, Z34, and Z35, respectively.

Furthermore, their energy levels are experimentally determined by photoemission yield spectroscopy (PYS). According to PYS result (Figure S1 b), the HOMO energy level of Z33 is -5.34 eV and Z35 is -5.42 eV, slightly lower than for spiro-OMeTAD (-5.22 eV),^[45] whereas the HOMO energy level of Z34 is -5.14 eV, higher than spiro-OMeTAD, as shown in Figure 2 b. Moreover, the optical band gap (E_g), calculated from the ab-

sorption onset wavelength ($E_g = 1240/\lambda_{\text{onset}}$) of the corresponding absorption spectrum, indicates that the E_g is 2.72, 2.71, and 2.81 eV for Z33, Z34, and Z35, respectively. The LUMO levels of HTMs are calculated to be -2.62, -2.43, and -2.61 eV, which are more positive than that of $\text{CH}_3\text{NH}_3\text{PbI}_3$ (-3.91 eV).^[46] These results are in agreement with the trend derived from DFT calculations. Thus, these three HTMs can not only act as the hole-transporting layer, but can also serve as an electron-blocking layer in the PSCs.

The steady-state photoluminescence (PL) spectra are shown in Figure 2 c. Strong PL quenching was observed when the HTM materials were coated on the perovskite films. For the three HTMs coated perovskite films, the PL intensity was reduced to roughly 26, 20, and 46% of the intensity obtained from pristine films for Z33, Z34, and Z35, respectively, suggesting that Z34 can extract charge carriers more efficiently than the other two HTMs. The hole extraction capacities of Z33–Z35 at the glass/ $\text{CH}_3\text{NH}_3\text{PbI}_3$ /HTM interfaces have been investigated by time-resolved photoluminescence (TRPL) measurement. Figure 2 d presents the measured PL decay spectra and the corresponding decay times are obtained by fitting the data with a biexponential decay function.^[47] The PL decay lifetime is reduced to 82.8, 63.1, 107.9, and 47.1 ns for devices with Z33, Z34, Z35, and spiro-OMeTAD

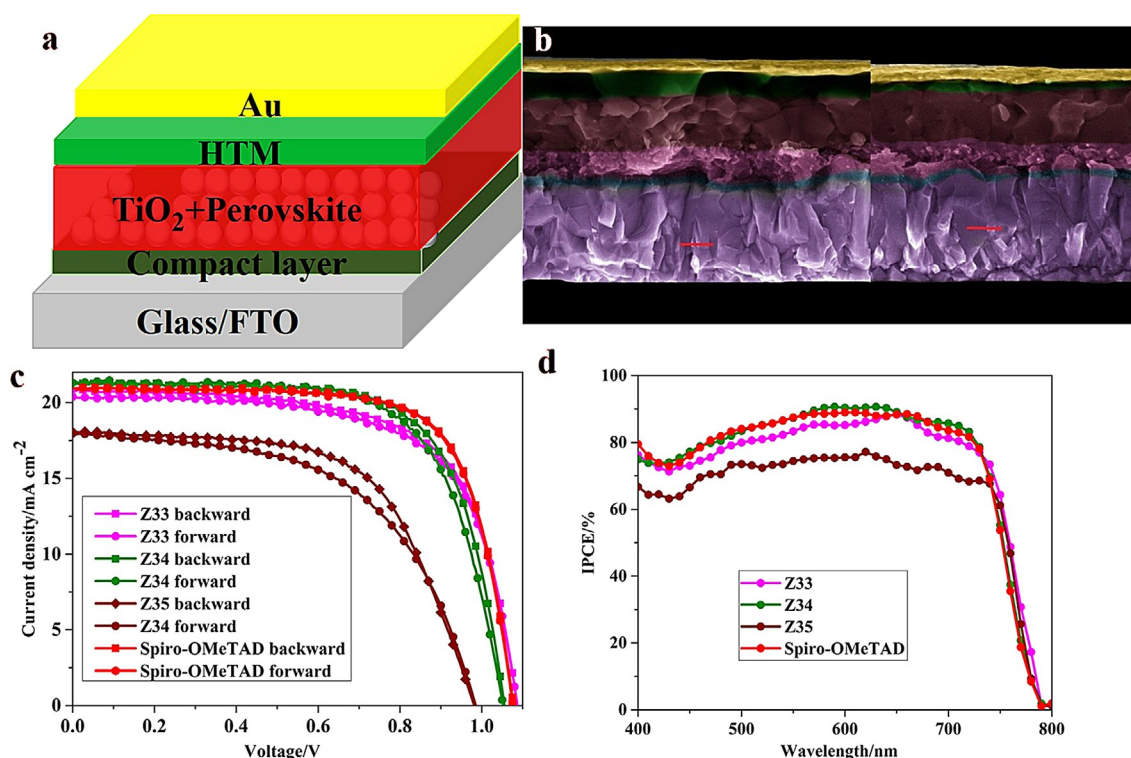


Figure 3. (a) Representation of photovoltaic device structure; (b) cross-sectional SEM image of the representative device, spiro-OMeTAD (left) and Z34 (right), the scale bar is 200 nm; (c) J - V hysteresis curves of PSCs comprising champion devices with HTMs measured starting with backward scan and continuing with forward scan; and (d) IPCE spectra of the devices based on Z33–Z35 without additives/dopants and spiro-OMeTAD with additives/dopants.

in comparison with 121.8 ns for the device without a HTM layer. From these observations, we conclude that hole injection from the valence band of perovskite into the HOMO of Z34 is more efficient than the other two HTMs.

A diagram of the PSCs applied in this study are shown in Figure 3a. The PSCs were fabricated by sequential deposition using a similar method as reported in our recent paper.^[48] Figure 3b presents a cross-sectional scanning electron microscopy (SEM) image of the PSC indicating clearly the infiltration of $\text{CH}_3\text{NH}_3\text{PbI}_3$ perovskite into the TiO_2 pores forming a perovskite/ TiO_2 nanocomposite that is covered by a perovskite capping layer.

We evaluated the photovoltaic performance of PSCs based on the three HTMs and spiro-OMeTAD with or without doping. The photocurrent density–voltage (J - V) curves under AM 1.5 G irradiation of 100 mW cm^{-2} are presented in Figure 3c and Figure S4a, and the photovoltaic parameters are summarized in Table 2. The average PCE of the devices based on three HTMs varies from 10.8% for Z35 to 15.9% for Z34. The lower performance shown by Z35 is mainly related to insufficient driving force for hole injection as a result of its deeper HOMO energy level (-5.42 eV) compared to the valence band of $\text{CH}_3\text{NH}_3\text{PbI}_3$ (-5.43 eV). As expected, Z33 gives a higher open-circuit voltage ($V_{\text{oc}} = 1.087 \text{ V}$) than spiro-OMeTAD (1.078 V) for the device, which is commensurate with its lower HOMO level, whereas Z34 gives a lower V_{oc} (1.055 V) than spiro-OMeTAD owing to its higher HOMO level. The best device based on Z34 affords a V_{oc} of 1.055 V, a short-circuit current density (J_{sc}) of

21.2 mA cm^{-2} , and a fill factor (FF) of 0.70, leading to a PCE of 16.1% under AM 1.5 G (100 mW cm^{-2}) illumination. This result is comparable to that of spiro-OMeTAD (16.7%) doped with lithium bis(trifluoromethylsulfonyl)imide (LiTFSI) and 4-*tert*-butylpyridine (tBP). However, devices based the new HTMs doped with LiTFSI and tBP exhibit lower photovoltaic performance compared to dopant-free HTMs, especially in terms of FF and J_{sc} . This is partly because the dopants that work well with spiro-OMeTAD may not be suitable for the new HTMs.^[49] More-

Table 2. Device parameters of PCEs under different scan directions.^[a]

HTM ^[b]	Scan direction	J_{sc} [mA cm^{-2}]	V_{oc} [V]	FF	PCE [%]
Z33	backward	20.525	1.087	0.66	15.4
	forward	20.386	1.087	0.66	15.2
	avg	20.456	1.087	0.66	15.3
Z33 + +	backward	12.978	0.984	0.33	4.4
	backward	21.245	1.055	0.70	16.1
	forward	21.295	1.051	0.68	15.7
	avg	21.270	1.053	0.69	15.9
Z34 + +	backward	15.100	0.935	0.47	6.7
	backward	18.073	0.981	0.61	11.3
	forward	17.968	0.985	0.55	10.2
	avg	18.020	0.983	0.58	10.8
Z35 + +	backward	16.369	0.939	0.48	7.7
	backward	16.692	0.881	0.25	3.9
spiro-OMeTAD + +	backward	20.932	1.078	0.72	16.7
	forward	20.940	1.076	0.72	16.5
	avg	20.936	1.077	0.69	16.6

[a] Bias step of 5 mV. [b] + + = samples include LiTFSI and tBP additives.

over, the dopants seem to have a negative impact on film morphology, which can be seen from the SEM image in Figure S5. Similar behavior was observed with other reports.^[11, 40] In the absence of dopants, spiro-MeOTAD-based devices generated a PCE of only 3.92% owing to significant lowering of the V_{oc} and FF compared to the doped devices. Hysteresis behavior is frequently observed in PSCs. Only small hysteresis was observed in the $J-V$ curves. The measured PCE differences $[(PCE_{backward} - PCE_{forward}) / PCE_{average} \times 100\%]$ are 1, 3, 10, and 1% and the stabilized power outputs are 15.2, 16.1, 11.2, and 16.6% for devices based on Z33, Z34, Z35, and spiro-OMeTAD, respectively (Figure S6), consistent with the obtained PCE.

Figure S4b shows the J_{sc} illumination intensity dependence of the PSC devices. As it can be seen, the J_{sc} scales linearly with light intensity (I_{inc}), that is, $J_{sc} \approx I_{inc} \alpha$; with the slope α of 1.00, 1.00, and 0.99 for Z33, Z34, and Z35, respectively. This proves that no non-linear effects like direct recombination of electrons and holes in the mixed layer or quenching of excitons by free carriers play a significant role.^[51] According to previous investigations, it can be inferred that the bimolecular recombination is very weak in these devices.^[49, 50–52]

The incident photon-to-electron conversion efficiency (IPCE) spectrum of the cell with the four different HTMs is presented in Figure 3d. The integrated current densities estimated from the IPCE spectra (20.30, 20.90, 17.96, and 20.80 mA cm^{-2} for Z33, Z34, Z35, and spiro-OMeTAD, respectively) are in good agreement with the J_{sc} values obtained from the $J-V$ curves. We fabricated batches of 10 cells each using the three HTMs and spiro-OMeTAD and demonstrate in Figure 4 excellent reproducibility by the narrow statistical distribution of the photovoltaic metrics.

We compared the stability of Z33–Z35 and spiro-OMeTAD-based PSCs by exposing them to ambient air at 30% relative humidity without encapsulation. The time evolution of the photovoltaic metrics is shown in Figure 5. Devices based on

Z33 and Z34 show a slight increase of the PCE, whereas the devices based on spiro-OMeTAD and Z35 decrease after 1000 h. The devices based on Z33 and Z34 exhibited a slight increase in the PCE, that might be a result of improved conductivity of the HTM after oxygen doping during the aging test, which can be seen in Figure S6. The devices based on Z33–Z35 exhibited improved stability, which was mainly attributed to their lack of doping additives.^[53, 54] As shown in Figure S8, the contact angles of Z33 (89.1°), Z34 (92.1°), and Z35 (85.0°) are larger than for doped spiro-OMeTAD (66.9°) reported by our recent paper.^[35] Larger contact angles indicate higher hydrophobicity of the film. The more hydrophobic nature of Z33–Z35 helps to expel moisture away from the perovskite film, which could also lead to enhanced device stability.

In summary, we synthesized three novel D- π -D- π -D conjugated HTMs (Z33, Z34, and Z35) with a simple low-cost synthetic procedure. The HOMO and LUMO energy levels of these MeOTPA derivatives are effectively tuned to match with perovskite by introducing electron-donating groups symmetrically linked with olefinic bonds as the π bridge, which is demonstrated by optical and electrochemical studies. The PSC based on undoped Z34 as the HTM affords an impressive PCE of 16.1%, which is comparable to that obtained employing the well-known p-doped spiro-OMeTAD. The devices based on Z33–Z35 obtained a higher stability after 1000 h stored in the dark than the device based on spiro-OMeTAD at room temperature aged in ambient air with 30% relative humidity without encapsulation. Moreover, the cost to produce these HTMs is around 1/10 the synthetic cost of spiro-OMeTAD. The introduction of these three novel HTMs with improved synthesis, lower cost, and excellent performance highlight their potential use in the future deployment of PSCs.

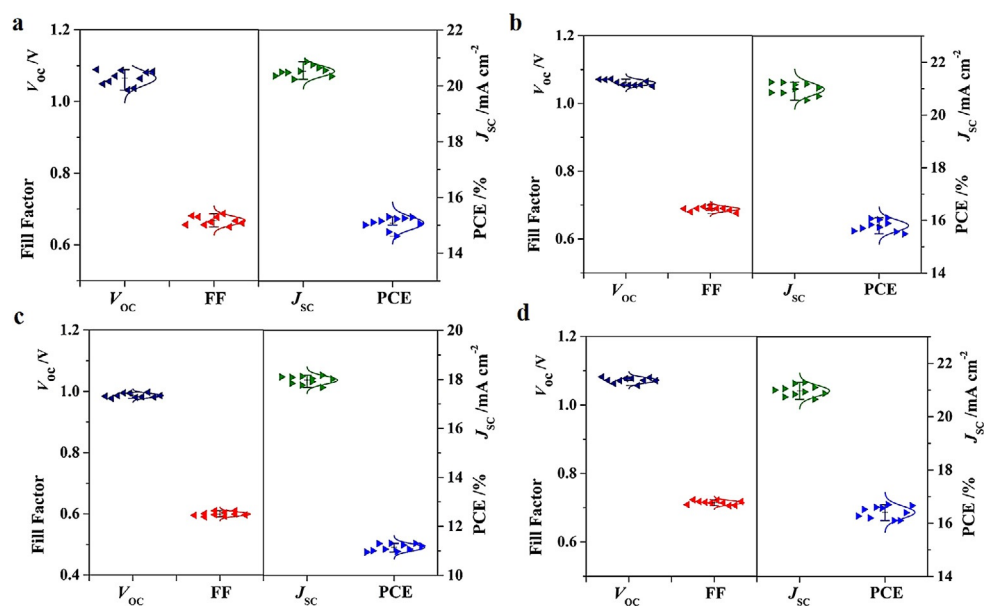


Figure 4. Statistical deviation of the photovoltaic parameters for 10 different solar cells using different HTMs: (a) Z33, (b) Z34, (c) Z35, and (d) spiro-OMeTAD.

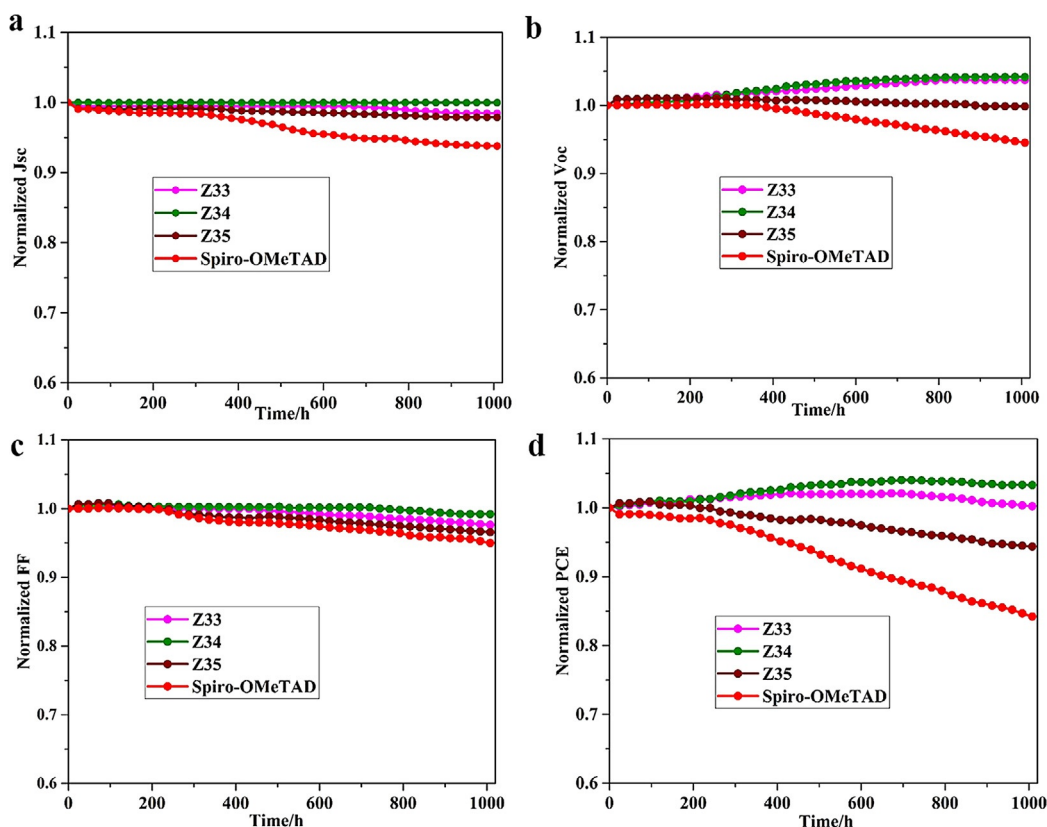


Figure 5. The stability of Z33–Z35 and spiro-OMeTAD-based PSCs in ambient air without encapsulation.

Experimental Section

Materials

Materials were all available commercially and used without further purification unless mentioned specially. Compound **2**, **3**, and **4** (Figure 1b) were synthesized according to our previous report.^[55]

Characterization

¹H NMR spectra were recorded with an INOVA 400 MHz spectrometer (Varian, USA). Mass spectra (MS) were performed on an Autoflex tof/tofIII mass spectrometer (Bruker, Germany). UV spectra of the HTMs in THF solutions ($1 \times 10^{-5} \text{ mol L}^{-1}$) were recorded with Thermo Evolution 300 UV/Vis spectrometer (Thermo Electron, USA) in the 200–800 nm wavelength range at room temperature. TGA were recorded with TA Q500 thermogravimetric apparatus (TA Instruments, USA) at a heating rate of $10^\circ\text{C min}^{-1}$ under nitrogen atmosphere. DSC was conducted on TA Q20 Instrument (TA Instruments, USA) at a heating rate of $10^\circ\text{C min}^{-1}$ under nitrogen atmosphere. PYS instrument was PYS-202 ionization energy test system (Sumitomo Heavy Industries, Japan) at the voltage of 100 V, waiting time of 1 s, and energy range from 4.0 to 8.5 eV. The time-of-flight (TOF) measurements were performed on TOF401 (Sumitomo Heavy Industries, Ltd. Japan), for which the samples were prepared through spin coating using a structure ITO/HTM (about $1 \mu\text{m}$)/Al (150 nm) with an active area of $3 \times 10 \text{ mm}^2$. The film thickness was performed on a surface profiler (P-6, KLA-Tencor, USA). The conductivities of the Z33- and Z34-based films were determined by using a two-contact electrical conductivity set-up following a previously reported procedure.^[56]

Synthesis of the HTMs

4-((E)-4-(di-*p*-tolylamino)styryl)-*N*-(4-((E)-4-(di-*p*-tolylamino)styryl)phenyl)-*N*-(4-methoxyphenyl)aniline (Z33): Compound **1** (0.17 g, 0.5 mmol) and **2** (1.26 g, 2 mmol) were added into a 100 mL round-bottom flask under N_2 . Anhydrous THF (40 mL) was added to the flask, and cooled to 0°C . A THF solution of *t*BuOK (16 mmol , 0.8 mol L^{-1}) was added dropwise to above flask and stirred for 30 min at 0°C , followed by stirring at room temperature until **1** was consumed completely (monitored by thin-layer chromatography). The reaction was quenched with ice water. The crude product was refluxed for 8 h in THF with a catalytic amount of iodine. Then the remaining iodine was removed using NaOH solution (10 wt%, 100 mL) with stirring for 2 h. After that, the product was purified using silica gel column chromatography (petroleum ether/ethyl acetate = 15:1 as eluent) to give the title compound as a pure compound Z33 (0.33 g, 77%): ¹H NMR (400 MHz, CDCl_3): $\delta = 7.32$ (t, $J = 8.1 \text{ Hz}$, 8H), 7.15–6.81 (m, 32H), 3.80 (s, 3H), 2.31 ppm (s, 12H); HRMS (m/z): 870.4403 [$M+H$], calcd, 869.4345; elemental analysis: found: C, 86.83; H, 6.36. Calc. for $\text{C}_{63}\text{H}_{55}\text{N}_3\text{O}$: C, 86.96; H, 6.37.

4-((E)-4-(bis(4-methoxyphenyl)amino)styryl)-*N*-(4-((E)-4-(bis(4-methoxyphenyl)amino)styryl)phenyl)-*N*-(4-methoxyphenyl)aniline (Z34): Z34 was prepared and purified according to the procedure described for Z33, starting from compound **3** (1.32 g, 2 mmol) and **1** (0.17 g, 0.5 mmol) to yield the desired product (0.32 g, 68%): ¹H NMR (400 MHz, CDCl_3): $\delta = 7.84$ (d, $J = 8.8 \text{ Hz}$, 1H), 7.68 (dd, $J = 12.0$, 7.3 Hz, 1H), 7.54 (d, $J = 6.2 \text{ Hz}$, 1H), 7.50–7.43 (m, 1H), 7.31 (dd, $J = 14.2$, 8.6 Hz, 6H), 7.16–6.76 (m, 30H), 3.80 ppm (d, $J = 5.2 \text{ Hz}$, 15H); HRMS (m/z): 934.4224 [$M+H$], calcd for $\text{C}_{63}\text{H}_{55}\text{N}_3\text{O}_5$:

933.4142; elemental analysis: found: C, 81.15; H, 5.94. Calc. for $C_{63}H_{55}N_3O$: C, 81.00; H, 5.93.

4-((E)-2-(9-ethyl-9H-carbazol-3-yl)vinyl)-N-(4-((E)-2-(9-ethyl-9H-carbazol-3-yl)vinyl)phenyl)-N-(4-methoxyphenyl)aniline (Z35): Z35 was prepared and purified according to the procedure described for Z33, starting from compound **4** (1.10 g, 2 mmol) and **1** (0.17 g, 0.5 mmol) to yield the desired product (0.25 g, 70%): $^1\text{H NMR}$ (400 MHz, CDCl_3): δ = 8.20 (s, 2H), 8.11 (d, J = 7.7 Hz, 2H), 7.64 (d, J = 8.4 Hz, 2H), 7.48–7.32 (m, 10H), 7.26–7.03 (m, 14H), 4.33 (dd, J = 14.2, 7.0 Hz, 4H), 2.34 (s, 3H), 1.42 ppm (t, J = 7.2 Hz, 6H); HRMS (m/z): Found 714.3481 [$M+H$], calcd, 713.3406; elemental analysis: found: C, 85.82; H, 6.08. Calc. for $C_{51}H_{43}N_3O$: C, 85.80; H, 6.07.

Solar cell fabrication

Devices were prepared on conductive fluorine-doped tin oxide (FTO)-coated glass substrates. The substrates were cleaned extensively with deionized water, acetone, and isopropanol. A compact TiO_2 layer was deposited by spray pyrolysis of 4.5 mL ethanol solution containing 0.3 mL titanium diisopropoxide bis(acetylacetonate) solution and 0.2 mL acetylacetone at 450 °C in air. On top of this layer, a 200–300 nm-thick mesoporous TiO_2 was formed by spin-coating 30 nm sized nanoparticles (30NRT, Dyesol) diluted in ethanol (1:6 w/w) at 5000 rpm for 20 s. The formed layer was heated to 500 °C and sintered for 0.5 h in oxygen atmosphere. The MAPbI_3 film was fabricated by sequential deposition using a similar method as developed by our recent paper.^[48] The lead iodide [PbI_2 , 1.2 M in a mixture of DMSO/*N,N*-dimethylformamide (DMF) 1:4 v/v] was spin coated on the top of the mesoporous TiO_2 layer at 4000 rpm for 10 s and left to dry for 10 min at 70 °C. Subsequently, 0.1 M MAI/isopropanol solution was sprayed and left for 90 s before spin coating at 3000 rpm for 10 s followed by drying at 100 °C for 1 h. Subsequently, for devices with spiro-MeOTAD and Z33–Z35 were dissolved in chlorobenzene at the concentrations of 72.3 mg mL⁻¹ [with 28.8 μL tBP and 17.5 μL of 520 mg mL⁻¹ LiTFSI acetonitrile solution dissolved in 1 mL chlorobenzene] and 20 mg mL⁻¹, respectively, and deposited on the perovskite layer by spin coating at 4000 rpm for 20 s. Devices were finalized by thermal evaporation of an 80 nm-thick gold layer.

Device measurement: To measure the J – V characteristics, the cells were illuminated under 100 mW cm⁻² (AM 1.5 G) by a 450 W Xenon lamp (Oriol), as a light source, equipped with a Schott K113 Tempax sunlight filter (Prazisions Glas&Optik GmbH) to match the emission spectra to the AM1.5G standard in the region of 350–750 nm. The J – V characteristics of the cells were recorded on Keithley (Model 2400) digital source meter. A mask with a window of 0.16 cm² was clipped to define the active area of the cell. The IPCE spectrum was obtained by focusing light from the 300 W Xenon lamp (ILC Technology, U.S.A.) through a Gemini-180 double monochromator (Jobin Yvon Ltd., U.K.) while chopping at 3 Hz before illuminating onto the photovoltaic cell.

Acknowledgements

We thank Dr. Gwénoél Jacopin (Laboratory of Quantum Optoelectronics, EPFL) for the PL test and Dr. Xiong Li (LPI, EPFL) for fruitful discussions. This work was supported by the Key Projects in Natural Science Foundation of Tianjin (16JCZDJC37100). F.Z. thanks the China Scholarship Council for funding. M.G. thanks

the King Abdulaziz City for Science and Technology (KACST) for financial support. Financial support from the Swiss National Science Foundation (SNSF), the NRP 70 “Energy Turnaround”, CCEM-CH in the 9th call proposal 906: CONNECT PV, the European Union’s Horizon 2020 research and innovation programme under the grant agreement No 687008 (GOTSolar) as well as from SNF-NanoTera and Swiss Federal Office of Energy (SYNERGY) is gratefully acknowledged. The information and views set out in this article are those of the author(s) and do not necessarily reflect the official opinion of the European Union. Neither the European Union institutions and bodies nor any person acting on their behalf may be held responsible for the use which may be made of the information contained herein.

Keywords: dopant-free · hole-transport material · perovskite · solar cells · stability

- [1] A. Kojima, K. Teshima, Y. Shirai, T. Miyasaka, *J. Am. Chem. Soc.* **2009**, *131*, 6050–6051.
- [2] F. Zhang, S. R. Wang, X. G. Li, Y. Xiao, *Curr. Nanosci.* **2016**, *12*, 137–156.
- [3] F. Zhang, S. R. Wang, X. G. Li, Y. Xiao, *Synth. Met.* **2016**, *220*, 187–193.
- [4] W. S. Yang, J. H. Noh, N. J. Jeon, Y. C. Kim, S. Ryu, J. Seo, S. I. Seok, *Science* **2015**, *348*, 1234–1237.
- [5] D. Q. Bi, W. Tress, M. I. Dar, P. Gao, J. S. Luo, C. Renevier, K. Schenk, A. Abate, F. Giordano, J. C. Baena, J. Decoppet, S. M. Zakeeruddin, M. K. Nazeeruddin, M. Grätzel, A. Hagfeldt, *Sci. Adv.* **2016**, *2*, e1501170.
- [6] M. Saliba, S. Orlandi, T. Matsui, S. Aghazada, M. Cavazzini, J. Correa-Baena, P. Gao, R. Scopelliti, E. Mosconi, K. Dahmen, F. D. Angelis, A. Abate, A. Hagfeldt, G. Pozzi, M. Grätzel, M. K. Nazeeruddin, *Nat. Energy* **2016**, *1*, 15017.
- [7] T. Swetha, S. P. Singh, *J. Mater. Chem. A* **2015**, *3*, 18329–18344.
- [8] Z. Yu, L. C. Sun, *Adv. Energy Mater.* **2015**, *5*, 1500213.
- [9] J. H. Heo, S. H. Kim, J. H. Noh, T. N. Mandal, C.-S. Lim, J. A. Chang, Y. H. Lee, H. Kim, A. Sarkar, M. K. Nazeeruddin, M. Grätzel, S. I. Seok, *Nat. Photonics* **2013**, *7*, 486–489.
- [10] B. Xu, E. Sheibani, P. Liu, J. Zhang, H. Tian, N. Vlachopoulos, G. Boschloo, L. Kloo, A. Hagfeldt, L. Sun, *Adv. Mater.* **2014**, *26*, 6629–6634.
- [11] L. Zheng, Y. H. Chung, Y. Ma, L. Zhang, L. Xiao, Z. Chen, S. Wang, B. Qu, Q. Gong, *Chem. Commun.* **2014**, *50*, 11196–11199.
- [12] J. A. Christians, R. C. M. Fung, P. V. Kamat, *J. Am. Chem. Soc.* **2014**, *136*, 758–764.
- [13] A. Krishna, D. Sabba, H. Li, J. Yin, P. P. Boix, C. Soci, S. G. Mhaisalkar, A. C. Grimsdale, *Chem. Sci.* **2014**, *5*, 2702–2709.
- [14] J. J. Guo, X. F. Meng, J. Niu, Y. Yin, M. M. Han, X. H. Ma, G. S. Song, F. Zhang, *Synth. Met.* **2016**, *220*, 462–468.
- [15] P. Qin, N. Tetreault, M. I. Dar, P. Gao, K. L. McCall, S. R. Rutter, S. D. Ogier, N. D. Forrest, J. S. Bissett, M. J. Simms, A. J. Page, R. Fisher, M. Grätzel, M. K. Nazeeruddin, *Adv. Energy Mater.* **2015**, *5*, 1400980.
- [16] J. W. Jung, C.-C. Chueh, A. K. Y. Jen, *Adv. Energy Mater.* **2015**, *5*, 1500486.
- [17] G. A. Sepalage, S. Meyer, A. Pascoe, A. D. Scully, F. Huang, U. Bach, Y. B. Cheng, L. Spiccia, *Adv. Funct. Mater.* **2015**, *25*, 5650–5661.
- [18] H. Li, K. Fu, A. Hagfeldt, M. Grätzel, S. G. Mhaisalkar, A. C. Grimsdale, *Angew. Chem. Int. Ed.* **2014**, *53*, 4085–4088; *Angew. Chem.* **2014**, *126*, 4169–4172.
- [19] H. Kim, K. G. Lim, T. W. Lee, *Energy Environ. Sci.* **2016**, *9*, 12–30.
- [20] K. G. Lim, H. B. Kim, J. Jeong, H. Kim, J. Y. Kim, T. W. Lee, *Adv. Mater.* **2014**, *26*, 6461.
- [21] P. Qin, S. Tanaka, S. Ito, N. Tetreault, K. Manabe, H. Nishino, M. K. Nazeeruddin, M. Grätzel, *Nat. Commun.* **2014**, *5*, 3834.
- [22] N. J. Jeon, J. H. Noh, W. S. Yang, Y. C. Kim, S. Ryu, J. Seo, S. I. Seok, *Nature* **2015**, *517*, 476.
- [23] M. Cai, V. T. Tiong, T. Hreid, J. Bell, H. Wang, *J. Mater. Chem. A* **2015**, *3*, 2784–2793.
- [24] J. Y. Xiao, L. Y. Han, L. F. Zhu, S. T. Lv, J. J. Shi, H. Y. Wei, Y. Z. Xu, J. Dong, X. Xu, Y. Xiao, D. M. Li, S. R. Wang, Y. H. Luo, X. G. Li, Q. B. Meng, *RSC Adv.* **2014**, *4*, 32918–32923.

- [25] S. T. Lv, Y. K. Song, J. Y. Xiao, L. F. Zhu, J. J. Shi, H. Y. Wei, Y. Z. Xu, J. Dong, X. Xua, S. R. Wang, Y. Xiao, Y. H. Luo, D. M. Li, X. G. Li, Q. B. Meng, *Electrochim. Acta* **2015**, *182*, 733–741.
- [26] M. Franckevicius, A. Mishra, F. Kreuzer, J. S. Luo, S. M. Zakeeruddin, M. Grätzel, *Mater. Horiz.* **2015**, *2*, 613–618.
- [27] S. Kazim, F. J. Ramos, P. Gao, M. K. Nazeeruddin, M. Grätzel, S. Ahmad, *Energy Environ. Sci.* **2015**, *8*, 2946–2953.
- [28] P. Qin, S. Paek, M. I. Dar, N. Pellet, J. Ko, M. Grätzel, M. K. Nazeeruddin, *J. Am. Chem. Soc.* **2014**, *136*, 8516–8519.
- [29] P. Qin, H. Kast, M. K. Nazeeruddin, S. M. Zakeeruddin, A. Mishra, P. Bäuerle, M. Grätzel, *Energy Environ. Sci.* **2014**, *7*, 2981–2985.
- [30] Y. K. Song, S. T. Lv, X. C. Liu, X. G. Li, S. R. Wang, H. Y. Wei, D. M. Li, Y. Xiao, Q. B. Meng, *Chem. Commun.* **2014**, *50*, 15239–15242.
- [31] J. J. Wang, S. R. Wang, X. G. Li, L. F. Zhu, Q. B. Meng, Y. Xiao, D. M. Li, *Chem. Commun.* **2014**, *50*, 5829–5832.
- [32] S. T. Lv, L. Y. Han, J. Y. Xiao, L. F. Zhu, J. J. Shi, H. Y. Wei, Y. Z. Xu, J. Dong, X. Xu, D. M. Li, S. R. Wang, Y. H. Luo, Q. B. Meng, X. G. Li, *Chem. Commun.* **2014**, *50*, 6931–6934.
- [33] L. F. Zhu, J. Y. Xiao, J. J. Shi, J. J. Wang, S. T. Lv, Y. Z. Xu, Y. H. Luo, Y. Xiao, S. R. Wang, Q. B. Meng, X. G. Li, D. M. Li, *Nano Res.* **2015**, *8*, 1116–1127.
- [34] Y. K. Wang, Z. C. Yuan, G. Z. Shi, Y. X. Li, Q. Li, F. Hui, B. Q. Sun, Z. Q. Jiang, L. S. Liao, *Adv. Funct. Mater.* **2016**, *26*, 1375–1381.
- [35] X. C. Liu, L. F. Zhu, F. Zhang, J. You, Y. Xiao, D. M. Li, S. R. Wang, Q. B. Meng, X. G. Li, *Energy Technol.* **2016**, DOI: 10.1002/ente.201600303.
- [36] X. Y. Liu, F. Zhang, X. C. Liu, M. N. Sun, S. R. Wang, D. M. Li, Q. B. Meng, X. G. Li, *J. Energy Chem.* **2016**, *25*, 702–708.
- [37] F. Zhang, C. Y. Yi, P. Wei, X. D. Bi, J. S. Luo, G. Jacopin, S. R. Wang, X. G. Li, Y. Xiao, S. M. Zakeeruddin, M. Grätzel, *Adv. Energy Mater.* **2016**, *6*, 1600401.
- [38] Y. S. Liu, Z. R. Hong, Q. Chen, H. J. Chen, W. H. Chang, Y. Yang, T. B. Song, Y. Yang, *Adv. Mater.* **2016**, *28*, 440.
- [39] C. H. Huang, W. F. Fu, C. Z. Li, Z. Q. Zhang, W. M. Qiu, M. M. Shi, P. Heremans, A. Jen, H. Z. Chen, *J. Am. Chem. Soc.* **2016**, *138*, 2528.
- [40] F. Zhang, X. M. Zhao, C. Y. Yi, D. Q. Bi, X. D. Bi, P. Wei, X. C. Liu, S. R. Wang, X. G. Li, S. M. Zakeeruddin, M. Grätzel, *Dyes Pigm.* **2016**, DOI: 10.1016/j.dyepig.2016.08.002.
- [41] S. Karthikeyan, M. Thelakkat, *Inorg. Chim. Acta* **2008**, *361*, 635–655.
- [42] I. Neogi, S. Jhulki, M. Rawat, R. S. Anand, T. J. Chow, J. N. Moorthy, *RSC Adv.* **2015**, *5*, 26806–26810.
- [43] P. Cusumano, S. Gambino, *J. Electron. Mater.* **2008**, *37*, 231–239.
- [44] D. Poplavskyy, J. Nelson, *J. Appl. Phys.* **2003**, *93*, 341–346.
- [45] D. Q. Bi, B. Xu, P. Gao, L. C. Sun, M. Grätzel, A. Hagfeldt, *Nano Energy* **2016**, *23*, 138–144.
- [46] T. Krishnamoorthy, F. Kunwu, P. P. Boix, H. Li, T. M. Koh, W. L. Leong, S. Powar, A. Grimdale, M. Grätzel, N. Mathews, S. G. Mhaisalkar, *J. Mater. Chem. A* **2014**, *2*, 6305–6309.
- [47] J. B. You, Z. R. Hong, Y. Yang, Q. Chen, M. Cai, T. B. Song, C. C. Chen, S. R. Lu, Y. S. Liu, H. P. Zhou, Y. Yang, *ACS Nano* **2014**, *8*, 1674–1680.
- [48] C. Y. Yi, X. Li, J. J. Luo, S. M. Zakeeruddin, M. Grätzel, *Adv. Mater.* **2016**, *28*, 2964.
- [49] Y. S. Liu, Q. Chen, H. S. Duan, H. P. Zhou, Y. Yang, H. J. Chen, S. Luo, T. B. Song, L. Dou, Z. R. Hong, Y. Yang, *J. Mater. Chem. A* **2015**, *3*, 11940–11947.
- [50] D. Gebeyehu, M. Pfeiffer, B. Maennig, J. Drechsel, A. Werner, K. Leo, *Thin Solid Films* **2004**, *451–452*, 29–32.
- [51] P. Schilinsky, C. Waldauf, C. J. Brabec, *Appl. Phys. Lett.* **2002**, *81*, 3885.
- [52] V. D. Mihailetschi, H. Xie, P. W. M. Blom, *Appl. Phys. Lett.* **2002**, *87*, 203502.
- [53] G. Xing, N. Mathews, S. Sun, S. S. Lim, Y. M. Lam, M. Grätzel, S. Mhaisalkar, T. C. Sum, *Science* **2013**, *342*, 344.
- [54] F. G. Zhang, X. C. Yang, M. Cheng, W. H. Wang, L. C. Sun, *Nano Energy* **2016**, *20*, 108–116.
- [55] W. Z. Gao, S. R. Wang, Y. Xiao, X. G. Li, *Dyes Pigm.* **2013**, *97*, 92.
- [56] H. J. Snaith, M. Grätzel, *Appl. Phys. Lett.* **2006**, *89*, 262114.

Received: July 7, 2016

Revised: August 16, 2016

Published online on August 25, 2016